Approximate solutions to droplet dynamics in Hele-Shaw flows

Yoav Green†

Harvard T.H. Chan School of Public Health, Boston, MA 02115, USA

For the past decade, the interaction force between droplets flowing in a Hele-Shaw cell has been modelled as a dipole. In this work, we use the recently derived analytical solution of Sarig *et al.* (*J. Fluid Mech.*, vol. 800, 2016, pp. 264–277) of a two-droplet system, which satisfies the no-flux condition at both droplet interfaces, and compare it to results of the dipole model, which does not satisfy the no-flux condition. Unfortunately, the recently derived solution is given in terms of infinite Fourier series, making any additional straightforward analysis difficult. We derive simple approximations for these Fourier series. We show that at large spacing the approximations for the interactions reduce to the expected dipole-like solution. We also provide a new lower limit for the velocity for the case of almost touching droplets. For the case of large spacing, the derivation is extended to arbitrary droplet numbers – including an infinite lattice. We present a new correction for the dispersion relation for the perturbations. We investigate the effect of the number of droplets in a lattice, *N*, on the resulting dynamics.

---

1. Introduction

Droplet dynamics in microfluidic Hele-Shaw cells has garnered much interest in the last decade due to the many applications to which it is relevant. Notably, they have much promise for large-scale automation of chemistry and biology microfluidic-based systems (Garstecki *et al.* 2004; Link *et al.* 2004; Stone, Stroock & Ajdari 2004; Joanicot & Ajdari 2005; Squires & Quake 2005; Pompano *et al.* 2011). No less important, these same microfluidic systems also provide a platform to research fundamental science such as the effect of capillary number, the flow rate ratio and more (Christopher *et al.* 2008; Belloul *et al.* 2009).

A decade ago, Beatus, Tlusty & Bar-Ziv (2006) showed that the dispersion relation of an infinite translating lattice of droplets in a Hele-Shaw microchannel was analogous to that of phonons in a static solid-state crystal (Kittel 1986). This dispersion relation was derived under the assumption that the flow around each droplet was like the classical potential flow around a cylinder and the interactions between

† Email address for correspondence: ygreen@hsph.harvard.edu

droplets were dipolar. It is well known in fluid mechanics that the superposition of uniform and single dipole flows gives the classical solution of a flow around a cylinder, which satisfies a no-flux condition at the surface (Landau & Lifshitz 1959; Currie 1974). By adding additional dipolar interactions, the no-flux condition at each droplet surface is violated. Yet the resulting dipole model described experiments remarkably well (Beatus *et al.* 2006), even at small spacing where it is expected to fail. Since then the dipole model has become the hallmark model used for the investigation of interactions for systems of two or more droplets (Champagne *et al.* 2010; Champagne, Lauga & Bartolo 2011; Liu, Goree & Feng 2012; Uspal & Doyle 2012*a*,*b*; Desreumaux *et al.* 2013; Shani *et al.* 2014), including a mean-field approach, as well as the effects of confinement (Beatus, Bar-Ziv & Tlusty 2007) and the formation of Burgers shock waves (Beatus, Tlusty & Bar-Ziv 2009) in a microfluidics channel.

Later, Beatus, Bar-Ziv & Tlusty (2012) justified that using an infinite amount of reflections would result in a *de facto* no-flux boundary condition (BC). However, their argument was limited to two droplets (Beatus *et al.* 2012): 'Unfortunately, generalizing the method of reflections for three droplets or more is too cumbersome, since it involves enumerating the reflections created by more than two surfaces.' Owing to its inherent complexity, this two-droplet infinite-sum reflection potential was never tested for the dynamics of two droplets. While it is not surprising that the dipole model works at very large spacing, one should ask: Why does the model work at intermediate spacing when one does not expect the interactions to be purely dipolar?

In contrast to these many-body works, Sarig, Starosvetsky & Gat (2016) recently studied the dynamics of a two-droplet system in a Hele-Shaw channel. There, they solved for the pressure field for two arbitrarily sized and arbitrarily spaced droplets. Using bipolar-cylindrical coordinates, they derived an analytical solution, for the pressure field and forces on the droplets, in terms of infinite Fourier series, that satisfies the no-flux BC. Unfortunately, while their solution is exact, its complicated form does not allow for any additional straightforward analysis, including derivation of zeroth- and first-order dynamical equations. Upon simple inspection, their solution does not appear to reduce to the dipole solution, as is expected at large spacing. In this work, we will show that indeed it does, and we derive a new approximation for small spacing.

This work will be divided into two: $N = 2$ droplets (§§ 2 and 4) and $N > 2$ droplets (§ 5). In § 2 we present a short summary of the work by Sarig *et al.* (2016), which introduces the Fourier series and the forces. In § 3 we derive approximations for the Fourier series terms for large and small spacing. We then analyse the interplay of the various forces and rationalize why the dipole model appears to be successful even at small spacing. In § 4 we derive the zeroth- and first-order equations governing the two-droplet dynamics, which includes a new term in the perturbation equation. In § 5 we generalize our approach, for large spacing, from $N = 2$ to any $N > 2$ system and analyse these $N > 2$ systems. Concluding remarks are given in § 6.

2. Two-droplet problem definition

In general, in Hele-Shaw channels, the spacing separating the two surfaces, $\tilde{h}$ (where tilde marks dimensional units), is much smaller than all other length scales in the system. If inertia is negligible, the in-plane velocities are related to the pressure via $\tilde{\boldsymbol{u}} = -(\tilde{h}^2/12\tilde{\mu}_F)\tilde{\boldsymbol{\nabla}}\tilde{p}$ and the in-plane pressure is determined by $\tilde{\nabla}^2\tilde{p} = 0$, where $\tilde{\mu}_F$ is the viscosity of the background fluid. To simplify to $\boldsymbol{u} = -\boldsymbol{\nabla}p$, the velocity is normalized by a characteristic velocity $\tilde{U}$, and the in-plane length scales are

normalized by an in-plane characteristic length (discussed later), $\tilde{L}$, such that the pressure scales as $12\tilde{\mu}_F \tilde{U} \tilde{L} \tilde{h}^{-2}$.

That low-Reynolds-number flows can be described by a potential formulation has been leveraged to simplify the mathematical analysis of otherwise complicated problems. Perhaps the most notable is the Saffman–Taylor fingering instability whereby a less viscous fluid is injected into a more viscous fluid and the interface is unstable to transverse perturbations, leading to the formation of large fingers (Saffman & Taylor 1958). The case of small droplets was also analysed, and it was shown that surface tension ensures that the droplets are circular and stable (Taylor & Saffman 1959; Tanveer 1986). However, larger droplets can also have non-circular geometries (Tanveer 1986; Green, Lustri & McCue 2017) (see the discussion regarding the extraordinary branch in Tanveer (1986)). In this work we shall consider only circular droplets, which are of interest to numerous applications (Pompano *et al.* 2011), and were considered in Sarig *et al.* (2016) whose results we are extending.

One final comment is in order on the relation between Hele-Shaw flows and potential flows. In this work, we will be using the results derived in Sarig *et al.* (2016), who solved the Laplace equation in bipolar-cylindrical coordinates for the flow field around two circular cylinders under the assumption of a Hele-Shaw cell. However, a similar solution has already been derived in potential flows without the assumption of bipolar coordinates. The Villat formula gives a closed-form solution to the flow field around two cylinders in terms of an integral (Crowdy, Surana & Yick 2007). Thus, the large- and small-spacing approximations derived in this work are perhaps relevant and their concepts can be extended in the context of the Villat formula.

Our system comprises two identical droplets, of radius R and viscosity $\tilde{\mu}_d$, confined in a Hele-Shaw cell of height h (see figure 1*a* for a schematic). The background fluid has a viscosity $\tilde{\mu}_F$ and far from the droplets it is assumed that the fluid moves with a uniform flow velocity of U_∞ in the $\hat{x}$ direction, which is aligned with the axis connecting the droplets' centres. The droplet's centres are separated by a spacing distance $a(t)$.

Sarig *et al.* (2016) solved the Laplace equation, for the pressure, while satisfying the no-flux condition. Rather than treating the force on the droplet to be point-like, as the dipole model does, they integrated the pressure around each of the circular droplets and calculated the applied force. Their solution allowed for two-dimensional (2D) streaming flows (lateral and perpendicular flows). In this work we focus on one-dimensional (1D) lateral flows with identical droplets, as this corresponds to realistic experimental and numerical set-ups (Beatus *et al.* 2006, 2007; Champagne *et al.* 2010; Liu *et al.* 2012). However, our approximations can also be extended to solve 2D problems.

When the flow is aligned with the axis between the two centres of mass ($\hat{x}$ direction), the non-dimensional force acting on the ith droplet is (Sarig *et al.* 2016)

$$F_i = F_s + F_{pressure} + F_{friction} + F_{int} = 0, \tag{2.1}$$

$$F_s = 4\pi A^2 (U_\infty - \dot{x}_i) Q_s, \tag{2.2}$$

$$F_{int} = 4\pi A^2 (\dot{x}_l - U_\infty) Q_{int}, \tag{2.3}$$

$$F_{pressure} = \pi R^2 U_\infty, \tag{2.4}$$

$$Q_s = \sum_{n=1}^{\infty} n \mathrm{e}^{-2n\tau_R} \coth(2n\tau_R), \quad Q_{int} = \sum_{n=1}^{\infty} n \mathrm{e}^{-2n\tau_R} \operatorname{csch}(2n\tau_R), \tag{2.5a,b}$$
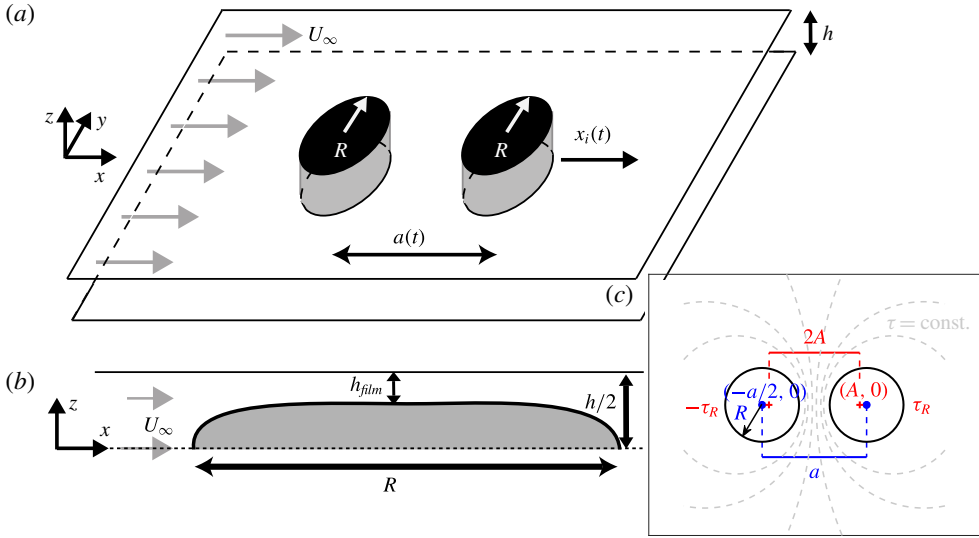
FIGURE 1. (Colour online) (*a*) Schematic description of the two-droplet set-up. The droplets are separated by a distance $a(t)$, confined between two plates separated by a distance h in the $\hat{z}$ direction, and have a radius R. The streaming velocity of the fluid is U_∞. The coordinate $\hat{x}$ is aligned along the axis line connecting the centres of the droplets. (*b*) Side view of a droplet in the channel. There is a thin film of fluid between the droplet and substrate with thickness h_{film}. (*c*) Top view of the droplets. The bipolar parameters A, τ_R (red markings) are related to a, R (blue markings).

where $i \neq l$ and $\dot{x}_i$ is the velocity of the ith droplet. Following Sarig *et al.* (2016), forces are normalized by $12\tilde{\mu}_F \tilde{U} \tilde{L}^2 \tilde{h}^{-1}$, where it is now obvious that $\tilde{L}$ can be either $\tilde{R}$ or $\tilde{a}$, and $\tilde{L} \gg \tilde{h}$. To avoid ambiguities when the spacing is infinite, $\tilde{L} = \tilde{R}$ is the preferred scaling. The bipolar cylindrical parameters A and τ_R will be discussed below. The droplet displacements can be written in the following manner:

$$x_i(t) = x_i(t=0) + U_d t + \delta x_i(t). \tag{2.6}$$

The third term is a perturbation term that describes small displacements about the leading-order translation term. It is assumed that the droplet velocities are identical. This need not be the case for non-symmetric droplets, as discussed in appendix A. The droplet spacing is

$$a = a(t) = x_i(t) - x_l(t) = a_0 + \delta x_i - \delta x_l = a_0 + \Delta\delta x, \tag{2.7}$$

where a_0 is the spacing at $t = 0$. The bipolar cylindrical parameters A and τ_R are related to a and R through the following relations (figure 1*c*) (Sarig *et al.* 2016):

$$A = \frac{\sqrt{a^2 - 4R^2}}{2} \approx \begin{cases} a/2, & a/R \gg 1 \text{ or } \tau_R \gg 1, \\ \sqrt{4\Delta\delta x R}, & A/R \ll 1 \text{ or } \tau_R \ll 1, \end{cases} \tag{2.8}$$

$$\tau_R = \sinh^{-1}\left(\frac{A}{R}\right) \approx \begin{cases} \log(a/R), & a/R \gg 1 \text{ or } \tau_R \gg 1, \\ A/R, & A/R \ll 1 \text{ or } \tau_R \ll 1. \end{cases} \tag{2.9}$$

The expressions for A and τ_R are approximated for large spacing, $\tau_R \gg 1$, and small spacing, $\tau_R \ll 1$. In this paper, the notation a/R and A/R appears often. While similar, these are not to be taken as the same. The notation $a/R \gg 1$ implies that the droplets are almost isolated, while the notation $A/R \ll 1$ implies that the droplets are almost touching such that $a_{min} = 2R$ (or $a/R \approx 2 + \Delta\delta x/R$). We note there is a difference in our notation of τ_R versus that of Sarig *et al.* (2016). In their work, $\tau_{1,2} = \pm\tau_R$ takes both positive and negative values (figure 1c). However, the Fourier coefficients (2.5) depend only on $|\tau_R|$. For brevity, we refer only to the absolute value (see appendix A and Sarig *et al.* (2016) for more details).

There are numerous forces that contribute to the governing equation (2.1). For the sake of clarity and brevity, from this point we distinguish only between the interaction term (2.3) and the direct term, which is the sum of all other terms

$$F_{direct} = F_s + F_{pressure} + F_{friction}. \tag{2.10}$$

The nomenclature direct and int for interaction will become more apparent in the next sections, where we will show that in the case of large spacing the direct force is independent of the spacing a_0 whereas the interaction term is a_0-dependent. The interaction term is the drag contribution due to the fact that there are two droplets. The pressure term accounts for a force due a pressure gradient in the channel and is reminiscent of a buoyant-like force.

We are finally left with modelling the frictional force. Beatus *et al.* (2006, 2007, 2009, 2012) modelled their friction force based on an energy argument where their friction coefficient, μ_{dipole} (not to be confused with the viscosity), had to be deduced for each experiment separately as the geometry and fluid properties were varied. In contrast, Sarig *et al.* (2016) suggested that the dimensional friction force was $\tilde{F}_{friction} = 12\pi\tilde{R}^2\tilde{U}_d\tilde{h}^{-1}(2\tilde{\mu}_d + \tilde{\mu}_F - 2\tilde{\mu}_F/\beta)$, where $\beta = U_d(a_0 \to \infty)/U_\infty$ is a parameter that is calibrated experimentally from a single isolated droplet. In non-dimensional form the friction force is (normalizing by $12\tilde{\mu}_F\tilde{U}\tilde{L}^2\tilde{h}^{-1}$)

$$F_{friction} = -\pi\eta R^2\dot{x}_i, \tag{2.11}$$

where the droplet velocity U_d has been replaced by $\dot{x}_i$ (2.6) and $\eta = \eta(\tilde{\mu}_F, \tilde{\mu}_d, \beta)$. One can consider (2.11) to be a general form for a non-dimensional friction where the exact details of $\eta = \eta(\tilde{\mu}_F, \tilde{\mu}_d, \beta)$ are not needed, nor are they currently known, which is why (2.11) is convenient. So rather than calibrating β one calibrates η. In fact, any function of the form $\tilde{F}_{friction} = 12\pi\tilde{R}^2\tilde{U}_d\tilde{h}^{-1}\tilde{\mu}_d\tilde{\beta}$ would eventually reduce to (2.11). Here we suggest another possible candidate for $\beta = U_d(a_0 \to \infty)/U_\infty$ based solely on scaling arguments. However, even here, some calibration is required.

First, consider the unperturbed Poiseuille flow in a Hele-Shaw cell. The shear stress scales as $\tilde{\mu}_F\tilde{U}_\infty\tilde{h}^{-1}$. This stress is integrated over a region proportional to $\tilde{R}^2$ yielding a force $\sim\tilde{\mu}_F\tilde{R}^2\tilde{U}_\infty\tilde{h}^{-1}$. Next, consider the well-studied case of a gaseous bubble in the channel, with zero contact angle, and a thin lubrication film separating the bubble and substrate (figure 1b). In the film, the viscous friction force scales as $\sim\tilde{\mu}_F\tilde{R}^2\tilde{U}_{film}\tilde{h}_{film}^{-1}$. Bretherton (1961) showed that the thickness of the film was $\tilde{h}_{film}/\tilde{h} = 2.38Ca^{2/3}$, where $Ca = \tilde{\mu}_F\tilde{U}_d/\tilde{\sigma}$ is the capillary number and $\tilde{\sigma}$ is the surface tension. This result was later generalized for the case of a viscous droplet and it was shown that the thickness could be increased by a factor of $2^{2/3}$ or $4^{2/3}$ depending on the viscosity ratio and boundary condition at the interface (Teletzke, Davis & Scriven 1988; Hodges, Jensen

& Rallison [2004]). If one assumes that the bottom interface moves with the droplet velocity, the force $\sim \tilde{\mu}_F \tilde{R}^2 \tilde{U}_d \tilde{h}^{-1} Ca^{-2/3}$. At sufficiently low Ca, h_{film} is independent of Ca and depends on the disjoining pressure such that $h_{film} = $ const. (Huerre *et al.* [2015]). This would change the dimensional formulation yet leaves the η formulation (2.11) unchanged. Indeed, further experiments are needed to determine the exact $\eta = \eta(\tilde{\mu}_F, \tilde{\mu}_d, \beta)$ relation as well as to determine whether or not there is any Ca dependence.

Prior to proceeding with further analysis, it is beneficial to consider the case when $O(\delta x_i)$ terms are negligible. Inserting (2.2)–(2.4), (2.6) and (2.11) into (2.1) yields the droplet velocity

$$U_d = \frac{4A^2(Q_s - Q_{int}) + R^2}{4A^2(Q_s - Q_{int}) + \eta R^2} U_\infty. \tag{2.12}$$

Note that we have still not approximated the Fourier series. We see that Q_s and Q_{int} are counteractive. The additional term in the numerator is the pressure, while in the denominator it is the friction. This equation is somewhat reminiscent of an equation given in Uspal & Doyle ([2012a]); however here we have only one coefficient η that needs to be calibrated from experiments, whereas Uspal & Doyle ([2012a]) had two coefficients (drag and friction) that needed to be determined from both experiments and phenomenological models.

3. Approximations

In this section we will approximate the coefficients of (2.5) for large ($\tau_R \gg 1$) and small ($\tau_R \ll 1$) spacing. We then compare these to the non-approximated terms.

3.1. *Large-spacing approximation*

The hyperbolic functions in (2.5) are approximated as $\coth(2n\tau_R) \approx 1 + 2e^{-4n\tau_R}$ and $\operatorname{csch}(2n\tau_R) \approx 2e^{-2n\tau_R} + 2e^{-6n\tau_R}$, yielding

$$Q_s^{(\tau_R \gg 1)} = \sum_{n=1}^{\infty} \frac{n(1 + 2e^{-4n\tau_R})}{e^{2n\tau_R}} = \frac{e^{2\tau_R}}{(e^{2\tau_R} - 1)^2} + \frac{2e^{6\tau_R}}{(e^{6\tau_R} - 1)^2} \approx \frac{R^2}{a^2} + \cdots, \tag{3.1}$$

$$Q_{int}^{(\tau_R \gg 1)} = \sum_{n=1}^{\infty} \frac{2n(e^{-2n\tau_R} + e^{-6n\tau_R})}{e^{2n\tau_R}} = \frac{2e^{4\tau R}}{(e^{4\tau R} - 1)^2} + \frac{2e^{8\tau R}}{(e^{8\tau R} - 1)^2} \approx 2\frac{R^4}{a^4} + \cdots. \tag{3.2}$$

We have kept only the leading-order terms after verifying that higher-order terms do not change the result. For large spacing, the direct and interaction forces are

$$F_{direct}^{(\tau_R \gg 1)} = [2U_\infty - (1 + \eta)\dot{x}_i]\pi R^2, \quad F_{int}^{(\tau_R \gg 1)} = 2\pi(\dot{x}_l - U_\infty)R^4/a^2. \tag{3.3a,b}$$

The direct force is spacing-independent. In contrast, it is clear that the interaction force is spacing-dependent with a dipolar behaviour. It should be stated here that the interaction is not set *a priori* to be dipolar, as in the potential approach (Beatus *et al.* [2012]), but rather it is a result.

3.2. *Small-spacing approximation*

For small spacing we employ the Poisson summation formula, where the sum of a series is given by (equation (8.7.33) in Prosperetti ([2011]))

$$\sum_{n=1}^{\infty} Q(n) = -\frac{1}{2} \lim_{x \to 0^+} Q(x) + \int_0^\infty Q(x)\, dx + 2\sum_{m=1}^{\infty} \int_0^\infty Q(x)\cos(2\pi m x)\, dx. \tag{3.4}$$

Inserting (2.5) yields

$$Q_s = \frac{\pi^2 - 4}{16\tau_R^2} - \frac{1}{4\tau_R} + \sum_{m=1}^{\infty} \left[\frac{\pi^2 m^2 - \tau_R^2}{2(\pi^2 m^2 + \tau_R^2)^2} + \frac{\pi^2}{8\tau_R^2} \operatorname{sech}^2 \left(\frac{\pi^2 m}{2\tau_R} \right) \right], \quad (3.5)$$

$$Q_{int} = \frac{\pi^2}{48\tau_R^2} - \frac{1}{4\tau_R} + \sum_{m=1}^{\infty} \left[\frac{1}{2\pi^2 m^2} - \frac{\pi^2}{8\tau_R^2} \operatorname{csch}^2 \left(\frac{\pi^2 m}{2\tau_R} \right) \right]. \quad (3.6)$$

Equations (3.5) and (3.6) are just another series representation of (2.5). However, in this representation it is more convenient to treat the case of $\tau_R \ll 1$, for it can be observed that the second expression in each sum goes to zero. In contrast, the first term is $\sum_{m=1}^{\infty} m^{-2} = \pi^2/6$. Interestingly, this sum will be encountered a number of times in this work. The coefficients reduce to

$$Q_s^{(\tau_R \ll 1)} = \frac{\pi^2 - 4}{16\tau_R^2} - \frac{1}{4\tau_R} + \frac{1}{12}, \quad Q_{int}^{(\tau_R \ll 1)} = \frac{\pi^2}{48\tau_R^2} - \frac{1}{4\tau_R} + \frac{1}{12}. \quad (3.7a,b)$$

The direct and interaction forces are

$$\frac{F_{direct}^{(\tau_R \ll 1)}}{\pi R^2} = (U_\infty - \dot{x}_i) \left(\frac{\pi^2 - 4}{4} - \tau_R + \frac{\tau_R^2}{3} \right) + U_\infty - \eta \dot{x}, \quad (3.8a)$$

$$\frac{F_{int}^{(\tau_R \ll 1)}}{\pi R^2} = (\dot{x}_l - U_\infty) \left(\frac{\pi^2}{12} - \tau_R + \frac{\tau_R^2}{3} \right). \quad (3.8b)$$

Inserting (3.8a) into (2.1) ($F_i = 0$) shows that the $O(\tau_R, \tau_R^2)$ terms identically cancel out.

Naturally the following questions arise: Is the small-spacing approximation physically and mathematically relevant? When the spacing is sufficiently small, will the Hele-Shaw approximation still hold? Will droplets also continue to remain circular? It is true that, under certain circumstances, the droplets can deform and no longer retain their circular shapes; however, this usually occurs for gaseous bubbles (Maxworthy 1986; Kopf-Sill & Homsy 1987). In contrast, it has been shown that one can create lattices of nearly touching circular droplets (Pompano *et al.* 2011) and it is often observed too that droplets do not deform. We will proceed under this assumption. For the case that the droplets are almost touching, the spacing is still much larger than the gap between the surfaces, $a_{min} = 2R \gg h$, so that the assumption of Hele-Shaw still holds. Further, Sarig *et al.* (2016) compared their theoretical model to the two-droplet experiments by Shen *et al.* (2014). The correspondence was striking, indicating that the Hele-Shaw approximation does not fail. Sarig *et al.* (2016) also made another prediction – that their model could be extended to the case of a smaller droplet encapsulated in a larger droplet. While this scenario is not discussed in this work, the Fourier coefficients for the scenario are almost the same as (2.5), thus the approximations derived in this work can, with some modifications, be used in the investigation of this alternative scenario.

3.3. *Approximation comparison*

We compare the large- and small-spacing models of the coefficients to the non-approximated terms (2.5) where it is evident that both the large- and small-spacing approximations correspond nicely to the non-approximated terms in each of their
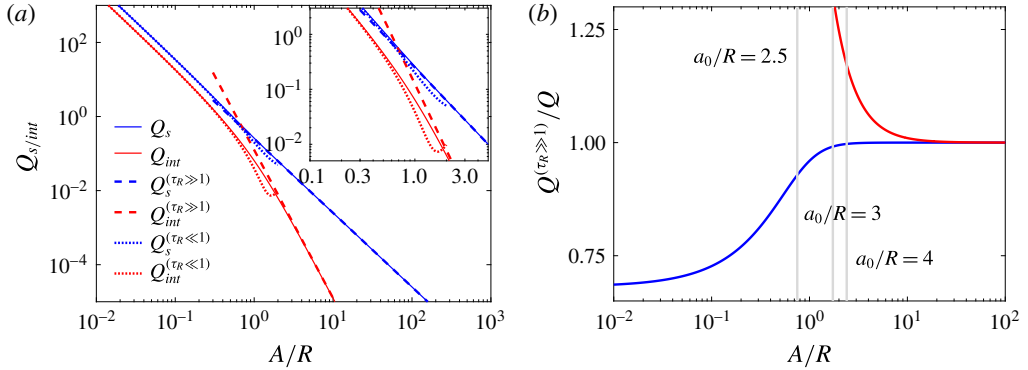
FIGURE 2. (Colour online) (*a*) Log–log plot of the various models of coefficients Q_s and Q_{int} versus A/R. (Inset) A zoom of (*a*). (*b*) Semi-log plot of the ratio of the large-spacing model to the exact model, $Q^{(\tau_R \gg 1)}/Q$, versus A/R ($Q_s^{(\tau_R \gg 1)}$, blue; $Q_{int}^{(\tau_R \gg 1)}$, red). The vertical grey lines mark $a_0/R = 2.5$, 3 and 4.

respective domains (figure 2*a*). It can be observed that for $A/R \gg 3$, $Q_s/Q_{int} \gg 1$, which indicates that the dynamics are primarily dictated by the direct term and not by the interaction term. In figure 2(*b*) we show that the large-scale approximation is valid for most of the A/R domain. We plot the ratio $Q^{(\tau_R \gg 1)}/Q$ versus A/R for both the *s* and int terms. It can be observed when $a_0/R \geqslant 3$ that the *s* ratio is unity while the int ratio departs slightly prior to that. Combined, these findings explain why the dipole model works well even at remarkably small spacing, such as $a_0/R = 4$, where one does not expect the dipole interaction assumption to hold.

4. Two-droplet velocity and perturbation equations

In this section we derive the zeroth-order equation, from which we calculate the droplet velocity, U_d, and the first-order correction for the perturbation dynamics.

4.1. *Large spacing*

The a^{-2} term in (3.3) can be rewritten (using (2.7)) as $a^{-2} \approx (1 - 2\Delta \delta x/a_0)a_0^{-2}$. Inserting this relation and (3.3) into (2.1) ($F_i = 0$) yields two equations of orders $O(1)$ and $O(\delta x/a_0)$, respectively:

$$U_d^{(\tau_R \gg 1)} = \frac{a_0^2 - R^2}{a_0^2(1 + \eta)/2 - R^2} U_\infty, \tag{4.1}$$

$$-\delta \dot{x}_i(1 + \eta) + 2\delta \dot{x}_l \frac{R^2}{a_0^2} = -4 \left[U_\infty - U_d^{(\tau_R \gg 1)} \right] \frac{R^2}{a_0^2} \frac{\Delta \delta x}{a_0}. \tag{4.2}$$

To compare with the dipole model, we derived the two-droplet velocity based on the dipole model formulation (Beatus *et al.* 2006, 2012). The results are similar; however, the $\delta \dot{x}_l R^2 a_0^{-2}$ term in (4.2) is new relative to the dipole model and is discussed later (§ 5.2). We also report an error in the reported expression for the velocity of an infinite lattice (discussed in § 5.2).

Finally, we recall that the parameter η needs to be calibrated experimentally relative to isolated droplets $U_d^{(\tau_R \gg 1)}(a_0 \to \infty) = 2U_\infty(1 + \eta)$. In this work we use
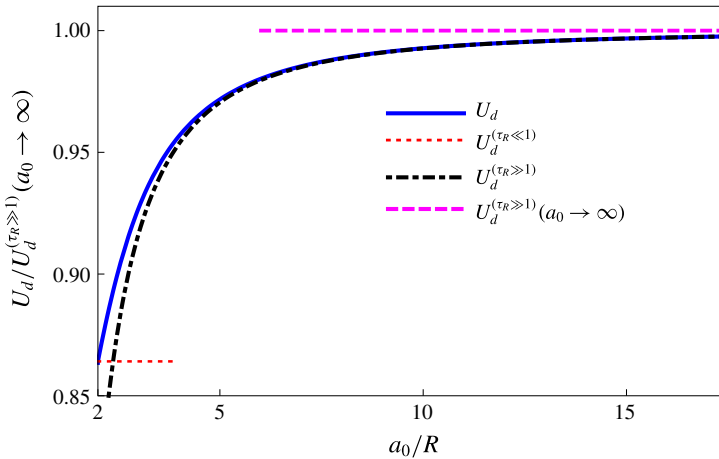
FIGURE 3. (Colour online) The droplet velocity, U_d, normalized by $U_d^{(\tau_R \gg 1)}(a_0 \to \infty)$, versus the normalized spacing a_0/R: $U_d^{(\tau_R \gg 1)}$ (4.1); $U_d^{(\tau_R \ll 1)}$ (4.3); U_d (2.12).

the experimental parameters given in figure 3 of Beatus *et al.* (2006), $\tilde{R} = 10$ µm, $\tilde{U}_d(a_0 \to \infty) = 295$ µm s^{-1} and $\tilde{U}_\infty = 1090$ µm s^{-1}, which yields $\eta = 2\tilde{U}_\infty/\tilde{U}_d - 1 \approx 6.36$.

4.2. *Small spacing*

Equation (2.1) yields two equations of order $O(1)$ and $O(\delta x R/A^2)$, respectively:

$$U_d^{(\tau_R \ll 1)} = \frac{\pi^2}{\pi^2 - 6 + 6\eta} U_\infty, \tag{4.3}$$

$$-3(4\eta + \pi^2 - 4)\delta \dot{x}_i + \pi^2 \delta \dot{x}_l = 0. \tag{4.4}$$

Equation (4.3) is a novel lower bound for the droplet velocity. Equation (4.4) has the trivial solution, $\delta x_i(t) = \delta x_i(t = 0)$, indicating that the droplet dynamics are quasi-stable.

4.3. *Droplet velocity comparison*

In figure 3 we plot the various models for the velocity as a function of droplet spacing. The non-approximated solution varies between the upper, $U_d^{(\tau_R \gg 1)}(a_0 \to \infty)$, and lower, $U_d^{(\tau_R \ll 1)}$, constant approximations. We see that the large-spacing approximation is valid for most spacing. This is no longer surprising, as discussed in § 3.3.

5. $N > 2$ **and infinite lattices**

5.1. *Extension from $N = 2$ to $N > 2$*

We know from Beatus *et al.* (2006) that, even when the no-flux BC is not satisfied, the dipole model corresponds very well to the experimental results for large spacing. In § 3.3, we showed that the effects of the interactions are not dominant if $a_0 \gg R$. This suggests that our $N = 2$ model can be extended to $N > 2$ where we acknowledge that such a system would not satisfy the no-flux BC. As we will show, the effects appear to be negligible. The extension of our mechanical equilibrium model to $N > 2$

droplet lattices using the superposition method is similar to the dipole model, yet our derivation differs in that we model the forces and do not use a predetermined velocity potential. An added advantage of our method is that in §4.1 we showed that our model predicts an additional term that does not exist in the traditional dipole model. We will analyse the effect of this term. In what will follow, we focus only on large spacing, $\tau_R \gg 1$, and for the sake of brevity and clarity, we drop all superscripts.

Our starting point is to require mechanical equilibrium such that each droplet satisfies $F_{direct} + F_{int,i}(N) = 0$. While F_{direct} is spacing- and N-independent (3.3), $F_{int,i}$ depends on both. Thus we rewrite the interaction force for the ith droplet to account for all interactions:

$$F_{int,i}(N) = \sum_{l \neq i}^{N} F_{int,i-l}. \tag{5.1}$$

To write out $F_{int,i-l}$ explicitly, we need to know the a_{il} spacings, which are given by

$$a_{il}(t) = a_{0,il} + \Delta\delta x_{\{i,l\}}, \tag{5.2}$$

$$a_{0,il}(t) = |i - l| \, a_0, \tag{5.3}$$

$$\Delta\delta x_{\{i,l\}} = \begin{cases} \delta x_i - \delta x_l, & i > l, \\ \delta x_l - \delta x_i, & i < l. \end{cases} \tag{5.4}$$

Equation (5.3) ensures that all the droplets are evenly spaced similar as in a solid-state crystal (Kittel 1986). Equation (5.4) ensures that the sign of the perturbation difference in (5.2) is self-consistent for each equation. In the interaction force, we are primarily interested in a_{il}^{-2}. The approximation yields

$$\frac{1}{a_{il}^2} \cong \frac{1 - 2\Delta\delta x_{\{i,l\}}/(a_0 |i - l|)}{a_0^2 (i - l)^2}. \tag{5.5}$$

As in §4, we shall need to divide the forces into zeroth- and first-order terms, which are denoted by the respective superscripts $O(1)$ and $O(\delta x)$:

$$F_{int,i-l}^{O(1)} = \frac{F_{2,l}}{(i - l)^2}, \tag{5.6}$$

$$F_{int,i-l}^{O(\delta x)} = \frac{2\pi R^4}{a_0^2 (i - l)^2} \delta\dot{x}_l - 2\frac{F_{2,l}}{(i - l)^2} \frac{\Delta\delta x_{\{i,l\}}}{a_0 |i - l|}, \tag{5.7}$$

where $F_{2,l} = 2\pi(U_{d,l} - U_\infty)R^4/a_0^2$ is the zeroth-order term of the two-droplet case (3.3). The subscript l indicates that this coefficient changes if one does not make the explicit assumption that the droplets move with a uniform velocity ($U_{d,l} = U_d$). Since an infinite lattice has a fore–aft symmetry, we make that assumption and drop this subscript, $F_{2,l} = F_2$.

5.2. *Infinite lattice*

In this section we shall reproduce the results of Beatus *et al.* (2006) for an infinite lattice. The zeroth-order expression from (5.1) yields

$$F_{int}^{O(1)}(N \to \infty) = \sum_{l=-\infty, l \neq i}^{\infty} F_{int,i-l}^{O(1)} = \sum_{l=-\infty, l \neq i}^{\infty} \frac{F_2}{(i - l)^2} = 2F_2 \sum_{l=1}^{\infty} l^{-2} = 2\left(\frac{\pi^2}{6}\right) F_2, \tag{5.8}$$

where we have already encountered this infinite sum. The zeroth-order force balance yields the velocity

$$U_d = \frac{a_0^2 - (\pi^2/3)R^2}{(1 + \eta)a_0^2/2 - (\pi^2/3)R^2} U_\infty. \tag{5.9}$$

Equation (5.9) has a similar form to (4.1) except that the R^2 coefficient is now $\pi^2/3$ instead of 1. Later, in figure 5, we compare the two-droplet case to the infinite lattice. It can be observed that, for a given spacing, the two-droplet system (solid grey line) has a higher velocity than the infinite lattice (solid black line). As the number of droplets increases, so does the number of interaction forces, resulting in an increase in the total interaction force, which operates as an effective drag. This results in a decrease of the velocity with increasing N, for constant spacing. This explanation and that $U_d(N = 2) > U_d(N \to \infty)$ conflict with the original 'peloton effect' explanation of Beatus *et al.* (2006, 2012) that compared the infinite lattice to riding cyclists. Indeed, cyclists riding in the turbulent wake of preceding cyclists can pedal less and stay at the same velocity; however, drag reduction is a large-Reynolds-number effect, related to boundary layer effects, that has no equivalent in classical low-Reynolds-number Hele-Shaw flows.

Equation (5.9) differs from that given in Beatus *et al.* (2006),

$$U_d^{(dipole)} = \frac{a_0^2 U_d^{(dipole,\infty)}}{a_0^2 + \pi^2 R^2(1 - U_d^{(dipole,\infty)}/U_\infty)/3}, \tag{5.10}$$

where $U_d^{(dipole,\infty)} = U_\infty(1 + \mu_{dipole}/\xi_d)^{-1}$ is the velocity of an isolated particle, μ_{dipole} is similar to our η, in the sense that it is a fitting parameter, and $\xi_d = \xi_d(\mu, R, h)$ was a drag parameter. Beatus *et al.* (2006, 2012) made an error in their final calculation. If one follows the derivation as prescribed in their works, one gets

$$U_d^{(corrected\ dipole)} = \frac{a_0^2 - (\pi^2/3)R^2}{a_0^2(U_\infty/U_d^{(dipole,\infty)}) - (\pi^2/3)R^2} U_\infty, \tag{5.11}$$

where it is now evident that (5.11) is similar in form to (5.9) when $a_0 \gg R$. In figure 5 we compare our infinite lattice (solid black line) and that of Beatus *et al.* (2006, 2012) (dashed black line). It is likely that Beatus *et al.* (2006, 2012) did not pick up their error because the functional forms of (5.9)–(5.11) are similar and matched experiments.

We now investigate the perturbation equations. Using $F_{int,i-l}^{O(\delta x)}$ (5.7) and $F_{direct}^{O(\delta x)}$ (3.3) yields

$$-(1 + \eta)\delta\dot{x}_i + \sum_{l=-\infty, l \neq i}^{\infty} \frac{2}{(i - l)^2} \left[\frac{\delta\dot{x}_l R^2}{a_0^2} - \frac{F_2 \Delta\delta x_{\{i,l\}}}{\pi R^2 a_0 |i - l|} \right] = 0. \tag{5.12}$$

This equation differs from the dipole model perturbation equation (Beatus *et al.* 2006, 2007, 2012), whereby our model includes the $\sum \delta\dot{x}_l$ coupling correction. For simplicity we neglect this term for now, as we reproduce the classical results of the dipole model. We shall add its effects hereafter. We rewrite (5.12) as

$$\delta\dot{x}_{\hat{i}=0} = -C_s \sum_{l=-\infty, l \neq 0}^{\infty} \frac{\Delta\delta x_{\{\hat{i}=0,l\}}}{|l|^3} = -C_s \sum_{l=1}^{\infty} \frac{\Delta\delta x_{\{0,l\}} + \Delta\delta x_{\{0,-l\}}}{l^3} = C_s \sum_{l=1}^{\infty} \frac{\delta x_l - \delta x_{-l}}{l^3}, \tag{5.13}$$

where $C_s = 4R^2(U_\infty - U_d)/[a_0^3(1 + \eta)]$. We insert a travelling wave, $\delta x_i \sim \exp[j(kx - \omega t)]$, into (5.13) ($j = \sqrt{-1}$ is the imaginary number). The droplet with subscript l is located at $x = la_0$. After some algebraic manipulations (5.13) yields

$$\omega_\infty = -2C_s \sum_{l=1}^{\infty} \frac{\sin(lka_0)}{l^3}. \tag{5.14}$$

The infinity subscript has been added to indicate an infinite lattice ($N \to \infty$). Equation (5.14) has the same form as that of the original work (Beatus *et al.* 2006, 2012) save for the fitting parameter η. We report that this infinite series converges to a simple polynomial of order 3 (see equation 1.443-5 on p. 47 of Gradshteyn & Ryzhik (2007)):

$$\sum_{l=1}^{\infty} \frac{\sin(lka_0)}{l^3} = \frac{\pi^2 ka_0}{6} - \frac{\pi(ka_0)^2}{4} + \frac{(ka_0)^3}{12}, \quad 0 \leqslant ka_0 \leqslant 2\pi. \tag{5.15}$$

Note that the coefficient of the linear term is the previously encountered $\pi^2/6$ similar to that in (3.5), (3.6) and (5.8) – the importance of which will become apparent soon. We return to the previously neglected coupling term in (5.12). Inserting the travelling wave into it yields

$$2\frac{R^2}{a_0^2} \sum_{l=-\infty, l\neq 0}^{\infty} \frac{\delta \dot{x}_l}{l^2} = -2j\omega e^{-j\omega t} \frac{R^2}{a_0^2} \sum_{l=1}^{\infty} \frac{e^{jkla_0} + e^{-jkla_0}}{l^2} = -j\zeta\omega e^{-j\omega t}, \tag{5.16}$$

where $\zeta = 2R^2[Li_2(jka_0) + Li_2(-jka_0)]a_0^{-2}$ is a real number, and $Li_2(\theta) = \sum_{l=1}^{\infty} \theta^l l^{-2}$ is the polylogarithm of order 2 and argument θ (Lewin 1991). Inserting (5.16) into (5.13) would modify (5.14) such that $\omega_{\infty,corrected} = \omega_\infty(1 + \eta)/(1 + \eta - \zeta)$. In figure 4 we plot the ratio $\omega_{\infty,corrected}/\omega_\infty$ for various values of a_0/R. Naturally, as the droplets are spaced farther apart, the correction is of less importance, yet, for closely packed droplets, the correction can be 4–6 %.

5.3. *The finite N-droplet lattice*

In the previous section we showed that the zeroth-order term of the total interaction force was multiplied by $\pi^2/3$ relative to the case of two droplets. We expect that this remains true also for a finite but large number of droplets. In reality, in a finite numbered lattice, the total interaction force on edge droplets is different from those near the centre. It can be shown that the ratio is at most a factor of 2. With this understanding, combined with the previous understanding, the interaction force is not the dominant force in the system; we make a simplifying assumption that all droplets behave as a droplet located at the centre. We shall show that, even for relatively small N, the lattice will behave in a very similar way to an infinite lattice. Hence we continue to require that $U_{d,i} = U_d$.

For the case of an odd number of droplets, $N = 2M + 1$ (M pairs relative to the central droplet), the total interaction force is straightforward:

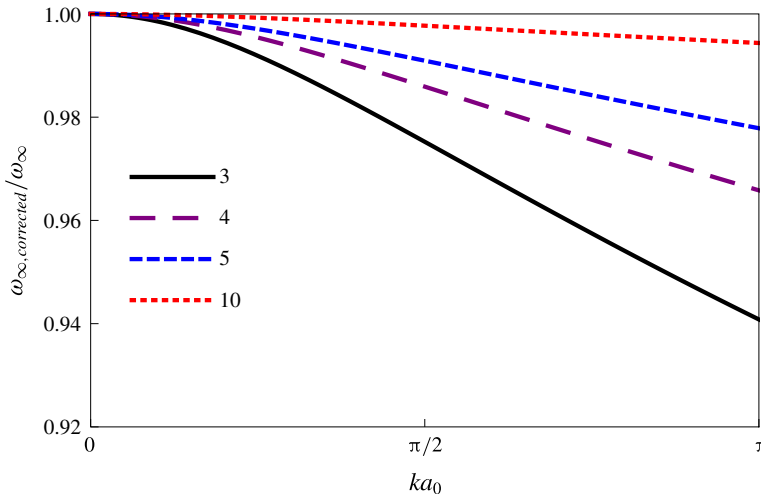$$F_{int}^{O(1)}(2N + 1) = 2F_2 \sum_{l=1}^{M} l^{-2} = G_M F_2, \tag{5.17}$$

FIGURE 4. (Colour online) Plot of $\omega_{\infty,corrected}/\omega_\infty$ versus the normalized wave number ka_0 for different a_0/R ratios and $\eta = 6.36$.

where $G_M = 2\sum_{l=1}^{M} l^{-2} = 2H_{M,2}$ and $H_{M,2}$ is the generalized harmonic number of order M of power 2. As can be expected, $H_{M\to\infty,2} \to \pi^2/6$. Like the infinite lattice, it can be shown that the droplet velocity is

$$U_d = \frac{a_0^2 - G_M R^2}{(1+\eta)a_0^2/2 - G_M R^2} U_\infty. \qquad (5.18)$$

Equation (5.18) has a similar form to (4.1) and (5.9). Already for small lattices ($G_{10}/G_\infty \sim 94\%$), the lattice is practically infinite and edge effects can be ignored.

In figure 5 we plot the droplet velocity versus the spacing for a travelling lattice of N droplets. As N increases, equation (5.18) varies monotonically from its $N = 2$ lower limit (4.1) to its $N \to \infty$ upper limit (5.9). As can be expected, already at $N = 21$ the lattice behaves as an almost infinite lattice, justifying the assumption $U_{d,i} = U_d$.

Similarly, the perturbation equation for finite N is

$$-(1+\eta)\delta\dot{x}_i + \sum_{l\neq i}^{2M+1} \frac{2}{(i-l)^2}\left[\frac{\delta\dot{x}_l R^2}{a_0^2} - \frac{F_2 \Delta\delta x_{\{i,l\}}}{\pi R^2 a_0 |i-l|}\right] = 0. \qquad (5.19)$$

For simplicity, we neglect the new correction term, which yields the following dispersion relation:

$$\omega_N = -2C_s \sum_{l=1}^{M} \frac{\sin(lka_0)}{l^3}. \qquad (5.20)$$

In figure 6(*a*) we plot the ratio $-\omega_N/2C_s$ versus the normalized wavenumber ka_0 for varying N. As the number of droplets increases, the solution converges to the infinite solution. It converges faster than the droplet velocity convergence because ω_N converges as l^{-3} while G_M converges as l^{-2}. It can be seen in figure 6(*b*) that $N = 3$ (two nearest-neighbour interactions) given by the dashed red line accounts for approximately 80 % of the ω_∞ response. Also, at relatively small numbers, such as
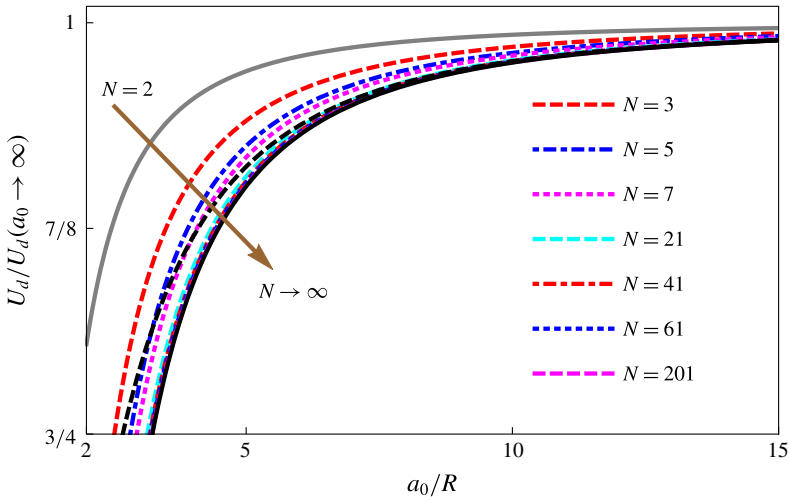
FIGURE 5. (Colour online) Normalized droplet velocity $U_d/U_d(a_0 \rightarrow \infty)$ versus a_0/R for varying number of droplets. The brown arrow points in the direction of increasing N. The two extreme cases of $N = 2$ (4.1) and $N \rightarrow \infty$ (5.9) are marked by a solid grey and black line, respectively. The black dashed line is the velocity (5.10) given by Beatus *et al.* (2006, 2012).
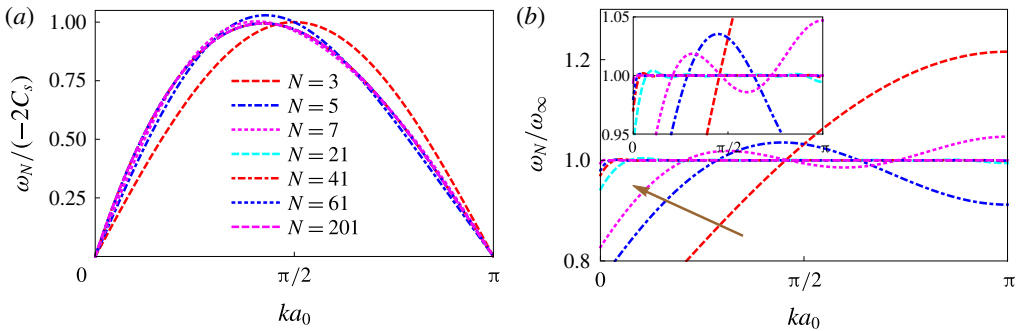

FIGURE 6. (Colour online) (*a*) A plot of $-\omega_N/2C_s$ versus the normalized wavenumber ka_0 for a system of varying droplet number, N. (*b*) A plot of the ratio ω_N/ω_∞ versus the normalized wavenumber ka_0. (Inset) A zoom of (*b*). The brown arrow indicates direction of increasing N.

$N \sim O(20)$, the ratio is unity for almost all ka_0. However, it can be observed that the solution does not converge at small ka_0 (large wavelengths) even for large N. This is rationalized based on a previous observation: the linear term of the dispersion relation (5.15) with the coefficient $\pi^2/6$ is determined by an infinite number of interactions. Simply put: a finite-sized lattice can sustain only a finite-sized wavelength.

6. Conclusions

In this work we have shown that using the large- and small-spacing approximations of the Fourier coefficients (2.5) allows the zeroth- and first-order governing equations to be written out in simple form. This allows for additional analysis that is not

possible with the non-approximated series. While this model recapitulates much of the results of the dipole model, it is different in that it does not use a predetermined flow potential and dictates the interaction to be dipolar. Rather, the dipolar interaction is a result. Further, the analysis is based on the assumption of mechanical equilibrium. Also, a new term, which does not exist in the dipole, appears. The discussion here follows the structure of this paper. We will first focus on the $N = 2$ findings and then move to the $N > 2$ findings.

In §3 we investigated the interplay between the various forces for $N = 2$ droplets. There, we showed that $Q_s \gg Q_{int}$, when $a_0/R > 3$, so that the effect of the interaction term is relatively negligible compared to the other forces such that dynamics are primarily determined by F_{direct}. We further show that the dipole model solution corresponds to the non-approximated velocity in most of the a_0/R domain, even at relatively small spacings where it is expected to fail (figure 3).

Thus far, the small-spacing approximation appears not to have received much attention in the literature. This is perhaps because it was assumed that if the interaction is not dipolar, the mathematical complexity increases, and perhaps that the Hele-Shaw approximation would fail. Sarig *et al.* (2016) compared their results with the experiments of Shen *et al.* (2014) and the correspondence was striking, indicating that the Hele-Shaw approximation holds. Further, our small-spacing solution provides a simple estimate, $U_d^{(\tau_R \ll 1)}$ (4.3).

Both the small- and large-spacing approximations have the potential to solve related problems. The formulation here can be extended to two dimensions, and/or can solve for non-identical droplets (Sarig *et al.* 2016). In appendix A we extend the large-spacing approximation for non-identical droplets. Also, Sarig *et al.* (2016) suggested that the model is also suitable for investigating the dynamics of a small droplet encapsulated in a larger droplet. The Fourier coefficients for such a scenario are almost the same as those discussed in this work. Hence, with some modifications, this too can be solved. These approximations can also be extended to investigate the well-known Villat formula. It would be interesting to see if that flow potential can be reduced to a simpler expression for large and small approximations.

The exact details of the friction coefficient are currently unknown. We have suggested a new form for the friction coefficient. It would be interesting and helpful to conduct a thorough experimental investigation of the velocity of an isolated drop $U_d(a_0 \to \infty)$ as a function of the parameters $U_\infty, R, h, \tilde{\mu}_f, \tilde{\mu}_d, \tilde{\sigma}$ as they are varied.

Finally, in §5 we extended the derivation from $N = 2$ to $N > 2$ droplets. For a given spacing, as N increases, U_d decreases. This is due to the increase of the effective drag. The velocity converges with increasing N to the infinite solution. For the dispersion relation, ω_N, we show that already at relatively small $N \sim O(20)$ the finite lattice behaves as an infinite lattice save for a small discrepancy at small ka_0. We also investigate the behaviour of the new $O(R^2/a^2)$ correction to the dispersion relation and show that it introduces a correction of a few per cent. In this work, we have started to investigate the effect of this term and we have shown that the new term leads to a few per cent change in the dispersion relation. Yet, it would indeed be interesting to see how this term might effect the long-time evolution of non-crystal-like lattices that have been investigated numerically and experimentally (Liu *et al.* 2012; Shen *et al.* 2014). It would indeed be interesting to investigate the case of a lattice of $N > 2$ where all droplets are touching. On the one hand, we know that all non-nearest-neighbour dynamics ($a_{ij} > 4R$) can be modelled by dipolar interactions, yet it is unclear how the nearest-neighbour interactions ($a_{min} = 2R$) should be modelled. This is left for future work.

Acknowledgements

Appendix A. Two-droplet generalizations

Sarig *et al.* (2016) solved the case of two droplets of arbitrary radii and viscosities. For this general case, the Q coefficients have a more complicated form:

$$Q_s = \sum_{n=1}^{\infty} n e^{-2n|\tau_i|} \coth[n(|\tau_i| + |\tau_l|)], \tag{A 1}$$

$$Q_{int} = \sum_{n=1}^{\infty} n e^{-n(|\tau_i| + |\tau_l|)} \operatorname{csch}[n(|\tau_i| + |\tau_l|)], \tag{A 2}$$

$$A = (2a)^{-1} \sqrt{[a^2 - (R_1 + R_2)^2][a^2 - (R_1 - R_2)^2]}, \tag{A 3}$$

$$\tau_{1,2} = \pm \sinh^{-1}(A/R_{1,2}). \tag{A 4}$$

For the case of large spacing, when $a \gg R_1 + R_2$ ($A = a/2$ and $|\tau_i| = \log(a/R_i)$):

$$Q_s^{(\tau_R \gg 1)} = \sum_{n=1}^{\infty} n e^{-2n|\tau_i|} \coth\left[n(|\tau_i| + |\tau_l|)\right] \approx \sum_{n=1}^{\infty} n e^{-2n|\tau_i|} = \frac{e^{2\tau_i}}{(e^{2\tau_i} - 1)^2} \approx \frac{R_i^2}{a^2}, \tag{A 5}$$

$$Q_{int}^{(\tau_R \gg 1)} = \sum_{n=1}^{\infty} n e^{-n(|\tau_i| + |\tau_l|)} \operatorname{csch}[n(|\tau_i| + |\tau_l|)] \approx \sum_{n=1}^{\infty} 2n e^{-2n(|\tau_i| + |\tau_l|)}$$
$$= \frac{2e^{2(|\tau_i| + |\tau_l|)}}{[e^{2(|\tau_i| + |\tau_l|)} - 1]^2} \approx \frac{2R_i^2 R_l^2}{a^4}. \tag{A 6}$$

From (A 5), it is apparent that the force associated with the Q_s term is unequal for each droplet, which will lead to $F_{direct,1} \neq F_{direct,2}$ such that the droplets move at different velocity ($U_{d,i} \neq U_d$). The friction force is also dependent on the radii and viscosity $F_{friction,i} = \pi \eta_i R_i^2 \dot{q}_i$. Inserting all these results into (2.1) will yield an algebraic set of equations for $U_{d,i}$.

REFERENCES

BEATUS, T., BAR-ZIV, R. & TLUSTY, T. 2007 Anomalous microfluidic phonons induced by the interplay of hydrodynamic screening and incompressibility. *Phys. Rev. Lett.* **99** (12), 124502.

BEATUS, T., BAR-ZIV, R. H. & TLUSTY, T. 2012 The physics of 2D microfluidic droplet ensembles. *Phys. Rep.* **516** (3), 103–145.

BEATUS, T., TLUSTY, T. & BAR-ZIV, R. 2006 Phonons in a one-dimensional microfluidic crystal. *Nat. Phys.* **2** (11), 743–748.

BEATUS, T., TLUSTY, T. & BAR-ZIV, R. 2009 Burgers shock waves and sound in a 2D microfluidic droplets ensemble. *Phys. Rev. Lett.* **103** (11), 114502.

BELLOUL, M., ENGL, W., COLIN, A., PANIZZA, P. & AJDARI, A. 2009 Competition between local collisions and collective hydrodynamic feedback controls traffic flows in microfluidic networks. *Phys. Rev. Lett.* **102** (19), 194502.

BRETHERTON, F. P. 1961 The motion of long bubbles in tubes. *J. Fluid Mech.* **10** (2), 166–188.

CHAMPAGNE, N., LAUGA, E. & BARTOLO, D. 2011 Stability and non-linear response of 1D microfluidic-particle streams. *Soft Matt.* **7** (23), 11082–11085.

CHAMPAGNE, N., VASSEUR, R., MONTOURCY, A. & BARTOLO, D. 2010 Traffic jams and intermittent flows in microfluidic networks. *Phys. Rev. Lett.* **105** (4), 044502.

CHRISTOPHER, G. F., NOHARUDDIN, N. N., TAYLOR, J. A. & ANNA, S. L. 2008 Experimental observations of the squeezing-to-dripping transition in T-shaped microfluidic junctions. *Phys. Rev.* E **78** (3), 036317.

CROWDY, D. G., SURANA, A. & YICK, K.-Y. 2007 The irrotational motion generated by two planar stirrers in inviscid fluid. *Phys. Fluids* **19** (1), 018103.

CURRIE, I. G. 1974 *Fundamental Mechanics of Fluids*. McGraw-Hill.

DESREUMAUX, N., CAUSSIN, J.-B., JEANNERET, R., LAUGA, E. & BARTOLO, D. 2013 Hydrodynamic fluctuations in confined particle-laden fluids. *Phys. Rev. Lett.* **111** (11), 118301.

GARSTECKI, P., GITLIN, I., DILUZIO, W., WHITESIDES, G. M., KUMACHEVA, E. & STONE, H. A. 2004 Formation of monodisperse bubbles in a microfluidic flow-focusing device. *Appl. Phys. Lett.* **85** (13), 2649–2651.

GRADSHTEYN, I. S. & RYZHIK, I. M. 2007 *Table of Integrals, Series, and Products*, 7th edn. Academic Press.

GREEN, C. C., LUSTRI, C. J. & MCCUE, S. W. 2017 The effect of surface tension on steadily translating bubbles in an unbounded Hele-Shaw cell. *Proc. R. Soc. Lond.* A **473** (2201), 20170050.

HODGES, S. R., JENSEN, O. E. & RALLISON, J. M. 2004 The motion of a viscous drop through a cylindrical tube. *J. Fluid Mech.* **501**, 279–301.

HUERRE, A., THEODOLY, O., LESHANSKY, A. M., VALIGNAT, M.-P., CANTAT, I. & JULLIEN, M.-C. 2015 Droplets in microchannels: dynamical properties of the lubrication film. *Phys. Rev. Lett.* **115** (6), 064501.

JOANICOT, M. & AJDARI, A. 2005 Droplet control for microfluidics. *Science* **309** (5736), 887–888.

KITTEL, C. 1986 *Introduction to Solid State Physics*. Wiley.

KOPF-SILL, A. R. & HOMSY, G. M. 1987 Narrow fingers in a Hele-Shaw cell. *Phys. Fluids* **30** (9), 2607–2609.

LANDAU, L. D. & LIFSHITZ, E. M. 1959 *Fluid Mechanics*. Pergamon.

LEWIN, L. 1991 *Structural Properties of Polylogarithms*. American Mathematical Society.

LINK, D. R., ANNA, S. L., WEITZ, D. A. & STONE, H. A. 2004 Geometrically mediated breakup of drops in microfluidic devices. *Phys. Rev. Lett.* **92** (5), 054503.

LIU, B., GOREE, J. & FENG, Y. 2012 Waves and instability in a one-dimensional microfluidic array. *Physical Review* E **86** (4), 046309.

MAXWORTHY, T. 1986 Bubble formation, motion and interaction in a Hele-Shaw cell. *J. Fluid Mech.* **173**, 95–114.

POMPANO, R. R., LIU, W., DU, W. & ISMAGILOV, R. F. 2011 Microfluidics using spatially defined arrays of droplets in one, two, and three dimensions. *Annu. Rev. Anal. Chem.* **4** (1), 59–81.

PROSPERETTI, A. 2011 *Advanced Mathematics for Applications*. Cambridge University Press.

SAFFMAN, P. G. & TAYLOR, G. 1958 The penetration of a fluid into a porous medium or Hele-Shaw cell containing a more viscous liquid. *Proc. R. Soc. Lond.* A **245** (1242), 312–329.

SARIG, I., STAROSVETSKY, Y. & GAT, A. 2016 Interaction forces between microfluidic droplets in a Hele-Shaw cell. *J. Fluid Mech.* **800**, 264–277.

SHANI, I., BEATUS, T., BAR-ZIV, R. H. & TLUSTY, T. 2014 Long-range orientational order in two-dimensional microfluidic dipoles. *Nat. Phys.* **10** (2), 140–144.

SHEN, B., LEMAN, M., REYSSAT, M. & TABELING, P. 2014 Dynamics of a small number of droplets in microfluidic Hele-Shaw cells. *Exp. Fluids* **55** (5), 1728.

SQUIRES, T. M. & QUAKE, S. R. 2005 Microfluidics: fluid physics at the nanoliter scale. *Rev. Mod. Phys.* **77** (3), 977–1026.

STONE, H. A., STROOCK, A. D. & AJDARI, A. 2004 Engineering flows in small devices: microfluidics toward a lab-on-a-chip. *Annu. Rev. Fluid Mech.* **36** (1), 381–411.

TANVEER, S. 1986 The effect of surface tension on the shape of a Hele-Shaw cell bubble. *Phys. Fluids* **29** (11), 3537–3548.

TAYLOR, G. & SAFFMAN, P. G. 1959 A note on the motion of bubbles in a Hele-Shaw cell and porous medium. *Q. J. Mech. Appl. Maths* **12** (3), 265–279.

TELETZKE, G. F., DAVIS, H. T. & SCRIVEN, L. E. 1988 Wetting hydrodynamics. *Rev. Phys. Appl.* **23** (6), 989–1007.

USPAL, W. E. & DOYLE, P. S. 2012*a* Collective dynamics of small clusters of particles flowing in a quasi-two-dimensional microchannel. *Soft Matt.* **8** (41), 10676–10686.

USPAL, W. E. & DOYLE, P. S. 2012*b* Scattering and nonlinear bound states of hydrodynamically coupled particles in a narrow channel. *Phys. Rev. E* **85** (1), 016325.